Mechanism and regeneration of sulfur-poisoned Mn-promoted calcined NiAl hydrotalcite-like compounds for C$_3$H$_6$-SCR of NO

Ling Zhao [ID] *[ab] and Mengdi Kang[a]

The selective catalytic reduction of NO with propene (C$_3$H$_6$-SCR) in the presence of SO$_2$ was investigated over a series of Mn-promoted calcined NiAl hydrotalcite-like compounds. The obtained 5% MnNiAlO catalyst exhibits superior NO conversion efficiency (95%) at 240 °C, and excellent sulfur-poisoning resistance. The possible reaction pathways of the catalytic process were proposed according to several characterization measurements. It is demonstrated that Mn-promoted NiAlO catalysts enhance the Brønsted acid sites and surface active oxygen groups, and improve the redox properties by the redox cycle (Ni^{3+} + Mn^{2+} ↔ Ni^{2+} + Mn^{4+}). Thus, the amount of the reaction intermediates is improved, and the reactivities between C$_x$H$_y$O$_z$ species and nitrite/nitrate species are promoted. Furthermore, in the presence of SO$_2$, the MnNiAlO samples can give rise to minor formation of sulfate and inhibit the competitive adsorption effectively due to their nitrite/nitrate species being more abundant and stable. Finally, regeneration was studied using *in situ* FTIR and the water washing method showed the best performance on the regeneration of S-poisoned catalysts.

[a]*School of Ecology and Environment, Inner Mongolia University, China. E-mail: nmzhl@hotmail.com*

[b]*Center for Environmental and Human Toxicology, Department of Physiological Sciences, College of Veterinary Medicine, University of Florida, USA*

1. Introduction

Among the many problems related to air pollution, nitrogen oxides (NO$_x$) from stationary and mobile fuel combustion sources, due to its ever-increasing environmental concerns and more serious harm, have attracted more and more attention from society.[1,2] The stringent environmental regulations require limiting NO$_x$ emissions and promote research into reducing or capturing NO$_x$. The selective catalytic reduction of NO$_x$ by hydrocarbons (HC-SCR), which can eliminate NO$_x$ and unburnt hydrocarbons simultaneously, is regard as an economical, effective and energy-saving technique for the removal of NO$_x$ from automotive exhaust gases,[3,4] and propylene has become the most widely used hydrocarbon.[5]

However, an inevitable problem of SCR is the deactivation of catalysts by SO$_2$, owing to its permanent existence in typical diesel fired exhausts.[6] Thus, it is important to develop environmental-friendly SCR catalysts with excellent resistance against SO$_2$ poisoning. In addition, a mechanistic investigation is highly desired to exploit new catalysts with high sulfur-resistance.

Metal oxide catalysts have attracted much attention due to their high specific surface area, acid–base bifunctionality, synergistic effects and memory effects.[7,8] In previous reports, hydrotalcite derivatives such as La–Mg–Al,[9] K/Mg–Al[10] and Co–Ce[11] all exhibited performance in NO removal. Xu *et al.*[12] recently reviewed the progress over hydrotalcite-derived NiTi mixed oxide in NO$_x$ removal by selective catalytic reduction with ammonia. However, the sulfur resistance of the hydrotalcite-based catalyst is rarely studied. Previous literature analyzed the competitive adsorption between SO$_2$ and NO. The deactivation mechanism of catalysts caused by SO$_2$ reflects on two aspects.[13–16] Zhang *et al.*[13] reported that SO$_2$ could react with reduction gas to form sulfate species which did not decompose at low temperature and finally deposited on the catalyst surface. Wu *et al.*[14] demonstrated that the active phase on catalyst was sulfated by SO$_2$ to form sulfate species, which competed with the formation of nitrogenous species. Crittenden, Li, and co-workers have also achieved great progress in the development of SCR catalysts with excellent sulfur-poisoning resistance.[15,16]

It has shown that the introduction of a metal adjuvant in the metal oxide can further improve the catalytic activity, selectivity and anti-poisoning properties of the original catalyst.[17] According to the reports, manganese oxides have attracted special attention owing to their different types of labile oxygen and oxidation states,[18] which are necessary and important for completing a catalytic cycle.[18,19] Moreover, a series of manganese-containing metal oxide catalysts also show a significant enhancement of catalytic activity at low temperature.[20] In brief, it is inevitable for the deactivation of catalysts caused by SO$_2$. Therefore, the regeneration for catalysts is a very important process during SCR method. However the effect of SO$_2$ on their generation and transformation, has not been systemically addressed.

Herein, we synthesized x% MnNiAlO catalysts and examined their against SO$_2$-poisoning performance in the C$_3$H$_6$-SCR reaction. The reaction mechanism was investigated by *in situ* FTIR. The regeneration methods of deactivated catalyst were selected and investigated. The poisoning mechanism was analyzed by FTIR, XPS and Py-FTIR.

2. Experimental

2.1. Catalyst preparation

NiAl and ZrNiAl hydrotalcite were fabricated by a urea hydrolysis method according to the previous study.[21] NiAl-based hydrotalcite precursors were prepared by hydrothermal method. Different proportions of Mn were loaded in the preparation process, followed by calcined to prepare catalyst samples of x% MnNiAlO. The x stands for the atomic number of Mn in the whole of Mn, Ni and Al. For example, 1% MnNiAlO indicates Mn : (Mn + Ni + Al) atomic ratio of 1 : 100.

2.2. Catalyst characterization

The powder X-ray diffraction (XRD) were manufactured by Rigaku D/max-γb X-ray diffractometer with a CuKα radiation ($λ$ = 1.5418 Å), operated at 40 kV and 100 mA. Thermogravimetry analysis (TGA) was rendered on a NETZSCH STA 409 PC/PG simultaneous thermal analyses from 30–1000 °C in flowing air atmosphere. FTIR and Pyridine chemisorption spectra were obtained on a VERTEX 70 infrared spectrometer. The morphology of the catalysts was characterized by virtue of scanning electron microscopy (SEM, S-4800, Japan). The X-ray photoelectron spectroscopy (XPS) experiments were undertaken on an ESCALAB XI photoelectron spectrometer with Al Kα radiation. Curve fitting was conducted by use of XPSPEAK 4.1 with a Shirley background. Hydrogen temperature programmed reduction (H$_2$-TPR) was carried out in a Quantachrome Chem-BET Pulsar TPR (p/n 02139-1). O$_2$-TPD experiments were started from 30–1000 °C with a heating rate of 10 °C min^{-1} under Ar flow. A mass spectrometer (Hiden HPR20) was used for on-line monitoring of the O$_2$-TPD effluent gas.

2.3. Catalytic performance test

The de-NO$_x$ efficiency of the C$_3$H$_6$-SCR catalysts was evaluated employing a fixed-bed quartz tube reactor with the effluent gas of NO detected by gas chromatograph. Samples of 200 mg were applied to evaluate the catalytic performance under the following conditions: 1000 ppm NO, 1000 ppm C$_3$H$_6$, 5 vol% O$_2$, He as balance, and the total gas flow rate was 100 mL min^{-1}, the GHSV was 30 000 h^{-1}. Before each experiment, the catalyst was heated to 350 °C under He stream and held for 1 h, and the activity measurement was carried out at the heating rate of 10 °C min^{-1} from 150 °C to 350 °C. The conversion of NO was calculated as follows:

$$\text{NO conversion} = ([\text{NO}]_{in} - [\text{NO}]_{out})/[\text{NO}]_{in} \times 100\% \quad (1)$$

2.4. *In situ* FTIR measurements

The *in situ* FTIR experiments were performed on a VERTEX 70 infrared spectrometer. Before each experiment, the sample was pretreated at 400 °C in helium gas atmosphere for 60 min to remove trace impurities. When not specified, the test gas conditions were: [O$_2$] = 5 vol%, [NO] = [C$_3$H$_6$] = [SO$_2$] = 1000 ppm, He was a balance gas.

2.5. Regeneration of deactivated catalysts

2.5.1. Water washing. The deactivated catalysts were regenerated by washing with deionized water. 1 g deactivated sample was washed in 20 mL aqueous solution under continuous stirring for 2 h. Then the catalyst was filtered and dried at 110 °C.

2.5.2. Thermal regeneration in air. The deactivated catalysts were placed in a quartz tube ($Φ$ 6 mm) by packing quartz in air. The regeneration experiments were carried out by heating the samples with a heating rate of 10 °C min^{-1} in air. Then the samples were heated at 500 °C for 2 h purging with the air.

3. Results and discussion

3.1. Catalytic test

The NiAlO and MnNiAlO catalysts were tested in C$_3$H$_6$-SCR with and without SO$_2$. The NO conversion results in the temperature range of 150–350 °C without SO$_2$ are shown in Fig. 1(A). In these experiments, the NO conversion changed with the reaction temperature increasing over all the samples. The NiAlO sample achieved the maximum NO conversion of 43% at 250 °C. For Mn doped samples, their activities improved obviously, as well as the temperature corresponding to the maximum NO conversion shifted to a lower temperature. The 5% MnNiAlO exhibited the best catalytic performance with NO conversion which promptly reached about 95% at 240 °C. When the Mn amount is increased above 5% and further to 7%, the activity is declined. This phenomenon is owing to the excessive deposition of Mn, which leads to the agglomeration. Hence, we selected the 5% MnNiAlO catalyst as the target catalyst for further investigation.

The effects of the SO$_2$ on catalytic activity was investigated over NiAlO and 5% MnNiAlO catalysts at 240 °C, and the results are shown in Fig. 1(B). After introduction of SO$_2$ (100 ppm), the catalysts exhibit different sulfur-poisoning resistant properties.
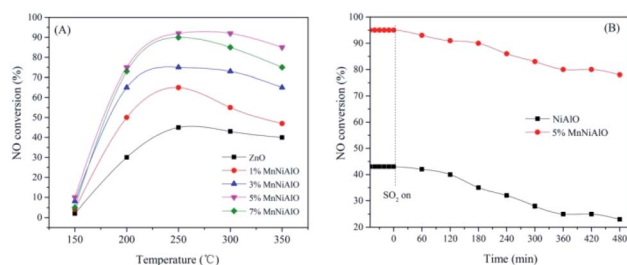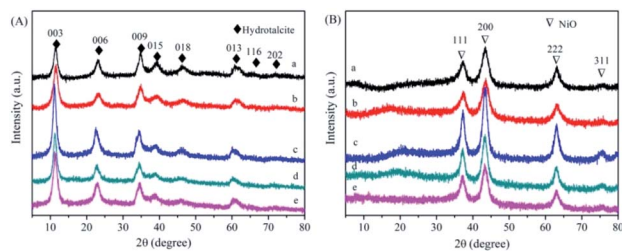

Fig. 1 (A) NO conversion as a function of temperatures over NiAlO and x% MnNiAlO catalysts. (B) NO$_x$ conversion of NiAlO and 5% MnNiAlO catalysts in the presence of 100 ppm SO$_2$ at 240 °C.

Fig. 2 (A) XRD patterns of NiA-HT and MnNiAl-HT precursor. (a) NiAl-HT precursor; (b) 1% MnNiAl-HT precursor; (c) 3% MnNiAl-HT precursor; (d) 5% MnNiAl-HT precursor; (e) 7% MnNiAl-HT precursor. (B) XRD patterns of NiAlO and x% MnNiAlO samples. (a) NiAlO; (b) 1% MnNiAlO; (c) 3% MnNiAlO; (d) 5% MnNiAlO; (e) 7% MnNiAlO.

Fig. 3 SEM images of NiAlO and 5% MnNiAlO catalysts calcined at 500 °C.

In terms of NiAlO sample, the NO_x conversion dropped significantly from 43% to 23% after 8 h. In contrast, the 5% MnNiAlO catalyst maintained high activity (from 95% to 88%) and excellent stability in the first 8 h, implying that Mn introduction could enhance NO_x reduction and maintain excellent catalytic activity in the presence of SO_2.
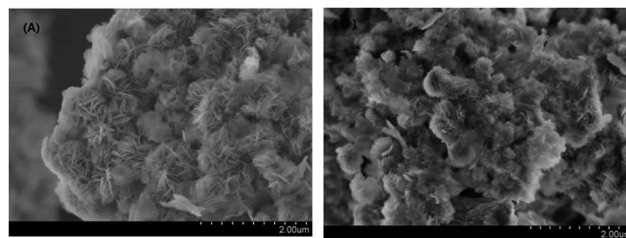
3.2. Morphology and physical properties of the catalysts

Fig. 2(A) shows the XRD spectra of NiAl-HT and four different Mn loadings samples. The characteristic peaks located at 11, 22, 35, 38, and 46° are assigned to the hydrotalcite structure (JCPDS 22-700).[22–24] Meanwhile, there are no additional peaks derived from Mn species for MnNiAl-HT samples, suggesting that Mn is well dispersed on the surface of the carrier. The unit cell parameters a and c of the hydrotalcite can be calculated assuming a 3R stacking sequence; therefore, $a = 2d_{110}$ and $c = d_{003} + 2d_{006} + 3d_{009}$, where the value of a is the average distance of two metal cations in adjacent unit cells and c is the interlayer distance regulated by the size and charge of the anion placed between the brucite-like layers. The structural parameters of the hydrotalcite-like samples are listed in Table 1. Both a and c remained unchanged with increasing Mn loading due to the ion radius disparity similarity between Ni^{2+} (56 Å) and Mn^{4+} (54 Å).

The XRD patterns of derived oxides (Fig. 2(B)) show the complete transformation from HT phase to oxide phase after calcination. The characteristic diffraction peak of the hydrotalcite disappeared, implying that the hydrotalcite structure collapses. Meanwhile, all samples show four distinctive peaks at about 37.4, 43.0, 63.4 and 75.2°, which are corresponding to the

NiO (111), (200), (220) and (311) crystal planes (JCPDS 47-1049), respectively. No diffraction peaks corresponding to crystalline Mn phase can be observed, due to the low Mn content or the high dispersion of Mn oxide.

SEM of NiAlO and 5% MnNiAlO catalysts is presented in Fig. 3. Two samples both exhibited pompon shape. Moreover, it can be found that the exposed crystal face of MnNiAlO was larger than NiAlO, which could provide more active sites for catalytic reaction.

The infrared spectra of NiAlO and x% MnNiAlO are shown in Fig. 4. The strong and wide absorption band located at 3484 cm^{-1} is attributable to the superposition of the stretching vibration between the interlayer H_2O and the layer-OH. The absorption band at 1648 cm^{-1} is attributed to the physically adsorbed water on the surface of the sample,[25] and the absorption band at 1384 cm^{-1} is attributed to CO_3^{2-}.[25] The absorption peak at 819 cm^{-1} is mainly caused by the vibration of the skeleton of the metal bond.

The H_2-TPR technology was employed in evaluating the reducibility of the catalysts. For all samples (Fig. 5), there are two reduction peaks centered at 675 °C and 780 °C. The former is related to the reduction of Ni species which has a low interaction with Al_2O_3 or small Ni particles, and the latter belongs to the reduction of a stable Ni^{2+} compound (NiO–Al_2O_3 or $NiAl_2O_4$ formed during calcination) which strongly reacts with Al_2O_3.[26] In the terms of x% MnNiAlO samples, they presented two new reduction peaks around 365 °C and 505 °C, although the peak signals were very weak. According to the previous literature, the

Table 1 Structural properties of the MnNiAl hydrotalcite

Sample	D-value				Lattice parameter	
	d_{003}	d_{006}	d_{009}	d_{110}	a	c
NiAl-HT	7.621	3.81	2.565	1.514	3.029	22.936
1% MnNiAl-HT	7.576	3.767	2.558	1.518	3.036	22.783
3% MnNiAl-HT	7.724	3.952	2.588	1.534	3.068	22.913
5% MnNiAl-HT	7.724	3.876	2.588	1.539	3.078	23.240
7% MnNiAl-HT	7.724	3.866	2.592	1.538	3.076	23.238
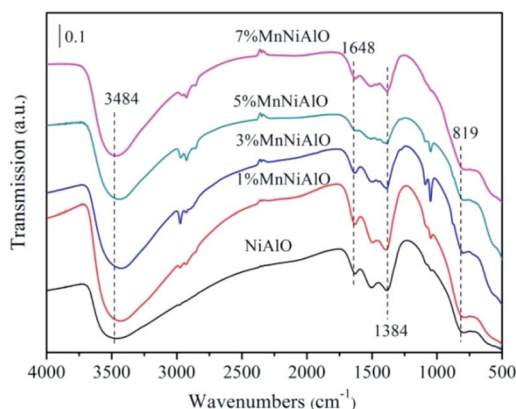
Fig. 4 FTIR spectra of the calcined NiAlO and MnNiAlO catalysts.
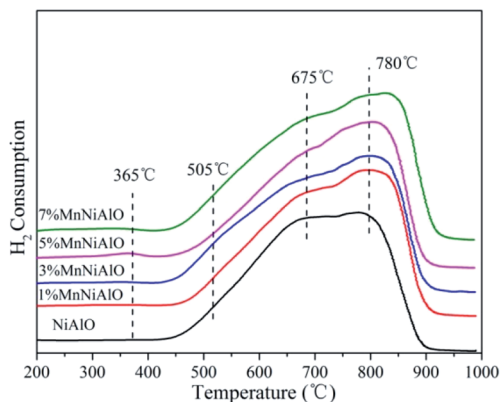
Fig. 5 H$_2$-TPR patterns of calcined NiAlO and MnNiAlO samples.

Fig. 6 O$_2$-TPD profiles of calcined NiAlO and MnNiAlO samples. (A) NiAlO; (B) 1% MnNiAlO; (C) 3% MnNiAlO; (D) 5% MnNiAlO; (E) 7% MnNiAlO.

two peaks can be attributed to the two-step reduction of MnO$_2$: the first step corresponds to the reduction of MnO$_2$ to Mn$_3$O$_4$, and the second step is the further reduction of Mn$_3$O$_4$ to MnO.[27] The total H$_2$ consumption increased at the same time as Mn-loading increased from 0 to 7 wt% as listed in Table 2, indicating that Mn doping can enhance the redox capacity of the samples, and finally accelerate the oxygen transfer and the oxidation process of NO to NO$_2$.

As shown in the O$_2$-TPD experiment (Fig. 6), three main characteristic peaks are clearly observed over each sample, which locate at 200–400 °C, 400–750 °C and above 750 °C, corresponding to the physically/chemically adsorbed oxygen O$_2$ (α), dissociated oxygen O^{2-}/O$^-$ at the vacancy sites (β), and bulk lattice oxygen (γ), respectively.[28] We also quantified the oxygen desorption peaks (Table 2), which suggested Mn incorporation obviously enhanced all the oxygen desorption peaks, especially the peak β, implying positive effects for the mobility of the active oxygen species of these catalysts. Besides, the physically/chemically adsorbed oxygen O$_2$ (α) and dissociated oxygen O^{2-}/O$^-$ at the vacancy sites (β) are found to be the most abundant over the 5% MnNiAlO catalyst, which reflect more active oxygen species. This is concordant with the catalytic test results (Fig. 1(A)). In fact, the first two kinds of oxygen species (α and β) are more crucial for the oxidation reaction during the C$_3$H$_6$-SCR.[4] It is beneficial to the oxidation following the steps C$_3$H$_6$ → C$_x$H$_y$O$_z$/carbonates (adsorption and oxidation) → CO/CO$_2$ (desorbed species).[4]

3.3. DRIFTS studies

3.3.1. Co-adsorption of NO + O$_2$. The *in situ* FTIR spectra of NO + O$_2$ on catalysts at 200 °C are presented in Fig. 7. As shown
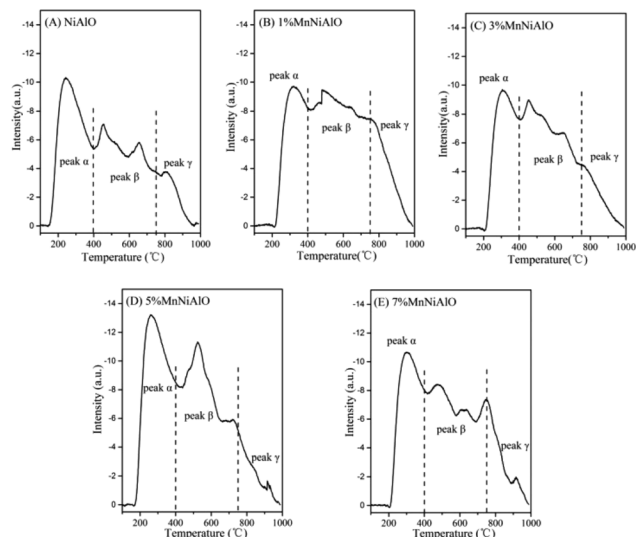
in Fig. 7(A), over NiAlO catalyst, nitrate species with different configurations appeared after introduction of NO/O$_2$ for 2 min, the bands at 1580 and 1349 cm^{-1} were assigned to adsorbed nitrate ion,[29] and the band at 1209 cm^{-1} was attributed to bridge bidentate nitrates.[29] The weak bands at 1449 and 1020 cm^{-1} belonged to *trans*-N$_2$O$_2$$^{2-}$ and bidentate nitrates, respectively.[30] Along with the time increasing, nitrate ion (1580, 1349 cm^{-1}) and bridging bidentate nitrate (1209 cm^{-1}) were pronounced at first and grew rapidly, and then decreased significantly over time. Meanwhile, *trans*-N$_2$O$_2$$^{2-}$ (1449 cm^{-1}) and bidentate nitrate (1020 cm^{-1}) increased continuously.[30] More important, monodentate nitrate species (1279 cm^{-1}) appeared after 10 min and accumulated greatly.[30] Taken together, we could infer the co-adsorption process of NO + O$_2$ on the catalyst surface. Firstly, NO was adsorbed onto the surface of the catalyst to form nitrate ion (1580, 1349 cm^{-1}), bridging bidentate nitrate (1209 cm^{-1}) and part of bidentate nitrate (1449, 1020 cm^{-1}). After the complete conversion of NO in the reaction cell, the absorption peaks of the bidentate nitrate species (1449 and 1020 cm^{-1}) still increased rapidly, whereas adsorbed nitrate ion species (1580 and 1349 cm^{-1}) gradually weakened. This indicates that the surface nitrate ion species could be transformed to bidentate nitrate over time. As the reaction progressed, the absorption peak of bridged bidentate

Table 2 The O$_2$ desorption peak area and total H$_2$ consumption of NiAlO and MnNiAlO catalysts

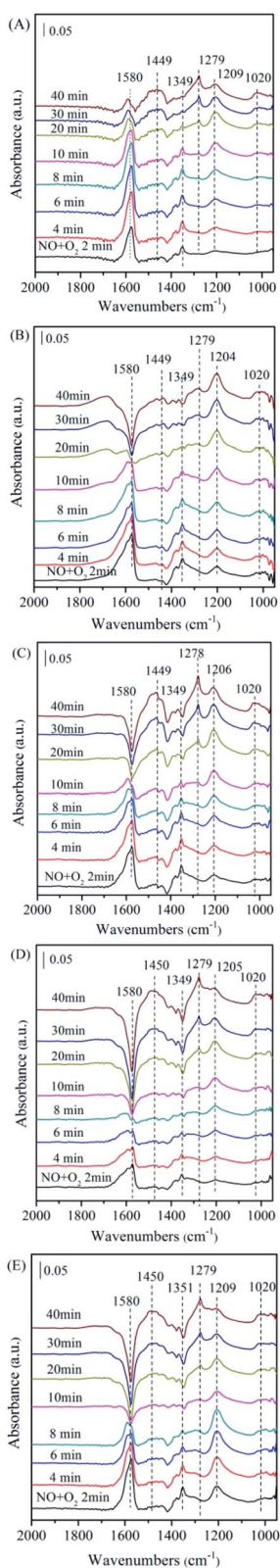| Sample	Peak α area (<400 °C)	Peak β area (400–750 °C)	Peak γ area (>750 °C)	Total area	Total H$_2$ consumption (µmol g^{-1})
NiAlO	1781.0	1897.3	505	4181.3	478.6
1% MnNiAlO	1365.6	2422.2	667.2	4455.0	574.9
3% MnNiAlO	1561.5	2485.2	513.8	4560.5	589.1
5% MnNiAlO	1866.7	2914.5	422.6	5203.8	704.6
7% MnNiAlO	1630.6	2594.8	498.6	5324.0	757.0

Fig. 7   The *in situ* FTIR spectra of the NiAlO and *x*% MnNiAlO catalysts reacting with NO + O$_2$ at 200 °C. (A) NiAlO; (B) 1% MnNiAlO; (C) 3% MnNiAlO; (D) 5% MnNiAlO; (E) 7% MnNiAlO.

nitrate (1209 cm^{-1}) gradually enhanced to the maximum value, after which bridged bidentate nitrate was decreasing accompanied by the appearance and strengthening of monodentate nitrate (1279 cm^{-1}). It is demonstrated that monodentate nitrate was converted from part of bridged bidentate nitrate.

In the case of MnNiAlO catalysts (Fig. 7(B)–(E)), the reaction process is basically similar to that of NiAlO catalyst. By comparing the adsorption amount of nitrogen-containing species, it can be concluded that the introduction of Mn into NiAlO sample promotes the adsorptive and active ability of catalyst for NO. This fact indicates that the synergetic effect between Ni and Mn facilitates the formation of different adsorbed NO$_x$ species. It is worth noting that for 7% MnNiAlO catalyst (Fig. 7(E)), its adsorbed NO species calculated by the band intensities were less than those of other MnNiAlO catalysts.

3.3.2.   Reactions between C$_3$H$_6$ and pre-adsorbed NO + O$_2$. In order to clarity the surface reactions and intermediates, the FTIR experiments in a flow of C$_3$H$_6$/O$_2$ after the catalyst was pre-adsorbed NO + O$_2$ followed by He purging at 200 °C were performed. In the case of NiAlO catalyst (Fig. 8(A)), NO and O$_2$ flushing at 200 °C produced adsorbed nitrate ion (1580 cm^{-1}), monodentate nitrate (1279 cm^{-1}), bidentate nitrates (1020 and 1482 cm^{-1}), and bridge bidentate nitrate (1209 cm^{-1}). A further switching the gas to C$_3$H$_6$ and O$_2$ led to a disappearance in nitrate ion and bridge bidentate nitrates, and also resulted in a decrease in monodentate nitrate species. This suggests that these adsorbed NO$_x$ species are active. Simultaneously, there is no significant change for bidentate nitrates (at 1020 and 1482 cm^{-1}), indicating that they were inert under this reaction condition. More important, the C$_x$H$_y$O$_z$ adsorbed species formed by adsorption of C$_3$H$_6$ (1574 and 1352 cm^{-1}) become
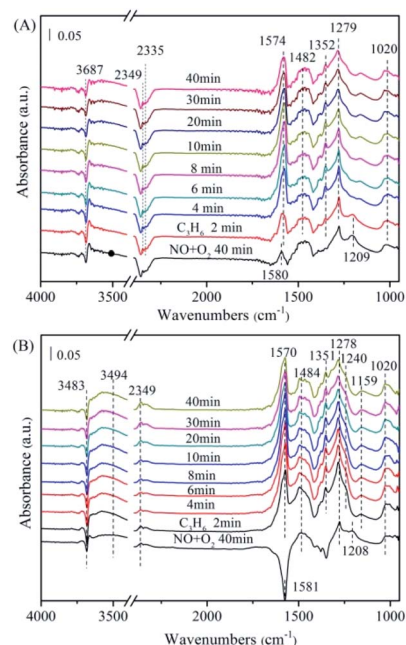

Fig. 8   The *in situ* FTIR spectra of the NiAlO and 5% MnNiAlO catalysts reacting with NO + O$_2$ and C$_3$H$_6$ at 200 °C. (A) NiAlO; (B) 5% MnNiAlO.

visible and accumulate considerably over time. The band recorded at 1574 cm^{-1} is assigned to formic acid or acetic acid.[31] The band at 1352 cm^{-1} belongs to carboxylate or enolic species (RCH=CH–O$^-$).[31] It is worth nothing that these surface $C_xH_yO_z$ adsorbed species grew rapidly within 10 min and then declined gradually, accompanied with a decrease in the signal of monodentate nitrate species (1279 cm^{-1}). Besides, a large amount for gas phase CO_2 was observed at 2335 cm^{-1} and 2349 cm^{-1}.[32] The peak at 3687 cm^{-1} is attributed to the ν (OH) stretching of adsorbed H_2O.[32] It is evident that the intensities of these bands are increased with time passing, implying some amount of CO_2 and H_2O are generated during the C_3H_6-SCR reaction process. This result is in agreement with previous work.[31] It is reported that the interactions of absorbed NO species and $C_xH_yO_z$ species are key steps for C_3H_6-SCR. $C_xH_yO_z$ amounts decreased by reaction with NO species and O_2 though carbonate species, directly gave rise to CO_2, N_2 and H_2O.

Fig. 8(B) displayed the FTIR spectrum of 5% MnNiAlO, respectively. The MnNiAlO catalyst exhibited the similar trend to NiAlO sample. The main species on the samples after NO/O$_2$ adsorption are nitrate ion (1581 cm^{-1}), monodentate nitrate (1278 cm^{-1}), bidentate nitrates (1020 and 1484 cm^{-1}), and bridge bidentate nitrates (1208 cm^{-1}). Switching to C_3H_6 atmosphere, the surface nitrate ion, bridge bidentate nitrate and monodentate nitrate species are observed to decline gradually. Surprisingly, the signal for chelating nitrite (at 1240 and 1159 cm^{-1}) were recorded at the same time, which differs from what occurs over NiAlO sample, suggesting the enhanced adsorption ability of NO on 5% MnNiAlO catalyst. General speaking, a higher NO conversion of one catalyst depends on a lower accumulation of adNO$_x$ and a stronger generation of $C_xH_yO_z$ species during C_3H_6-SCR. Compared to NiAlO catalyst, Mn doping samples showed much more concentration of $C_xH_yO_z$ surface species, which is indeed advantageous to the further deNO$_x$ process. This phenomenon may be due to the excellent redox and oxygen storage/release ability of Mn that can strongly activate adNO$_x$ for conversion, which is correlated to the H$_2$-TPR and O$_2$-TPD results (Fig. 5 and 6). Additionally, by comparing the amount of CO_2 and H_2O produced, it can be judged that Mn incorporation promoted the reactivity of $C_xH_yO_z$ species with nitrite/nitrate species, decomposing to more CO_2, N_2 and H_2O. These results are consistent with C_3H_6-SCR catalytic test (Fig. 1(A)).

3.4. SO$_2$ poisoning experiments

It is known that flue gas contains SO_2, the sulfate species with S=O bond can be formed on the surface of catalyst.[33] Moreover, SO_2 competes with NO for active sites to form sulfate species, thereby reducing the activity of catalyst. Meanwhile, SO_2 can react with the reducing gas for poisoning catalyst. Thus, we infer the poisoning mechanism for (Mn)NiAlO catalysts as follows. SO_2 mainly affects C_3H_6-SCR process through the following two aspects: one is the adsorption and activation of SO_2 on the surface of catalyst competes with adsorption and activation of NO. The other is the reaction between sulfate/sulfite and C_3H_6 competes with the reaction between nitrate/nitrite and C_3H_6. Both 5% MnNiAlO and

NiAlO catalysts are selected to compare their sulfur poisoning situation.

The FTIR experiments in a flow of NO/O$_2$ after the catalyst pre-adsorbed SO$_2$/O$_2$ were performed and the results were presented in Fig. 9. In the case of NiAlO sample (Fig. 9(A)), the catalyst surface was mainly covered by sulfite (at 1035 cm^{-1}),[34] sulfate (at 1165, 1243 and 1340 cm^{-1})[35,36] and molecular water (at 1601 cm^{-1}) after SO$_2$/O$_2$ adsorption. These species were bound to the catalyst surface strongly as the subsequent N$_2$ purging couldn't change their intensity of absorption bands. Switching to NO/O$_2$, no significant adsorbed NO$_x$ species could be detected, indicating that SO_2 competes with NO to adsorb over the NiAlO catalyst and occupies active sites preferentially through forming sulfite and sulfate species.

For 5% MnNiAlO catalyst (Fig. 9(B)), introduction of SO$_2$/O$_2$ resulted in the appearance of less sulfate species according to reducing the peak intensity of sulfate (at 1156 and 1245 cm^{-1}) compared with NiAlO sample. It is demonstrated significant decline of sulfate formation on 5% MnNiAlO sample. The results infer adding Mn could protect the active site of catalysts and improve resistance of catalysts towards SO_2. Herein, we think there are two reasons to explain this phenomenon. (i) Mn loading inhibits the formation of sulfate; (ii) the sulfate species formed on MnNiAlO present lower thermal stability and easier to be decomposed. Subsequently under NO/O$_2$ atmosphere, the peaks intensities of 1032, 1156 and 1245 cm^{-1} were increased obviously due to forming bidentate nitrate, chelating nitrite and monodentate nitrate, respectively, which differ from what occurs over NiAlO catalyst. This is clearly observed the absorbed NO species were generated much greater over SO$_2$-poisoned MnNiAlO catalyst than over SO$_2$-poisoned NiAlO. Based upon these results, it can be indicated that Mn addition gives rise to minor formation of sulfate after exposure to SO_2 and improves the resistance of catalyst towards SO_2. Moreover, the competitive adsorption phenomenon is dramatically inhibited over MnNiAlO samples due to their nitrite/nitrate species are more abundant and stable in comparison to NiAlO catalyst.

3.5. Regeneration of SO$_2$-poisoned catalysts

3.5.1. Thermal regeneration. After pre-adsorption of SO$_2$, the catalysts were heated and regenerated at 400 °C. The infrared spectrum of the reaction of NiAlO and 5% MnNiAlO catalyst with NO + O$_2$ and C$_3$H$_6$ after thermal regeneration is

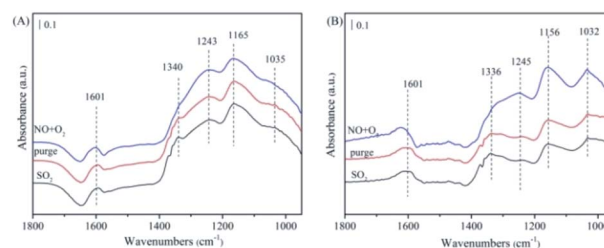**Fig. 9** The FTIR spectra of the catalysts with pre-adsorbed SO$_2$/O$_2$ upon exposing in NO/O$_2$, followed by C$_3$H$_6$/O$_2$ at 200 °C. (A) NiAlO; (B) 5% MnNiAlO.

shown in Fig. 10. In the term of NiAlO sample (Fig. 10(A)), the absorption peaks belonging to sulfates (1160 and 1341 cm^{-1}) decreased, while the absorption peaks belonging to sulfites (1032 and 1240 cm^{-1}) increased after regeneration, which proves that the method of thermal regeneration could not reduce the amount of sulfate adsorbed on the surface of the catalyst. This phenomenon may be due to the fact that thermal regeneration converts partially unstable adsorbed sulfate into SO$_2$ at 400 °C and some SO$_2$ is quickly activated to form a more thermally stable sulfate species adsorbed on the catalyst, resulting in more severe clogging. After introduction of NO/O$_2$, there is no absorption peak attributed to nitrate. After passing into C$_3$H$_6$, no change was observed in any peak. These results suggest that the thermal regeneration method could not regenerate the catalytic activity of NiAlO sample.

In the case of 5% MnNiAlO (Fig. 10(B)), the results were the same as those presented in the previous discussion. After thermal regeneration at 400 °C, the peaks of sulfite (1032 cm^{-1}) and some sulfates (1160 cm^{-1}) decreased, whereas that of sulfate at 1338 cm^{-1} increased slightly. The result demonstrated that after high-temperature regeneration, the 5% MnNiAlO catalyst had fewer types of sulfate species and smaller quantities than the NiAlO catalyst. After passing NO/O$_2$, the absorption peaks at 1032 and 1156 cm^{-1} were enhanced, which were attributed to the presence of bidentate nitrate species. In addition, the absorption peak at 1240 cm^{-1} moved toward a low wavenumber because of the formation of a monodentate nitrate. After passing through C$_3$H$_6$, no change was observed in any peak. This proved that for the 5% MnNiAlO catalyst, thermal regeneration could partially restore the activation and adsorption capacity of NO but could not restore the reaction ability of C$_3$H$_6$ with these produced nitrogen oxides.

3.5.2. Water washing regeneration. After pre-adsorption of SO$_2$, the catalysts were regenerated by water washing. The infrared spectrum of the reaction of NiAlO and 5% MnNiAlO catalyst with NO + O$_2$ and C$_3$H$_6$ after washing regeneration is shown in Fig. 11. For the NiAlO catalyst (Fig. 11(A)), after washing regeneration, the peaks of sulfite (1031 cm^{-1}) and sulfates (1168 and 1245 cm^{-1}) reduced, whereas that of sulfate at 1340 cm^{-1} maintained stable. Moreover, a new absorption peak at 1425 cm^{-1} is attributed to sulfate. This phenomenon may be due to the fact that during the washing process, part of the sulfate is washed away, whereas partially unstable adsorbed sulfate is converted into SO$_2$ and then some SO$_2$ is quickly
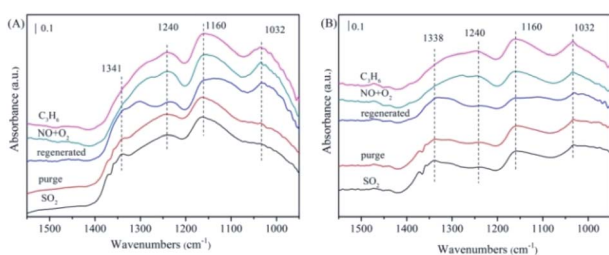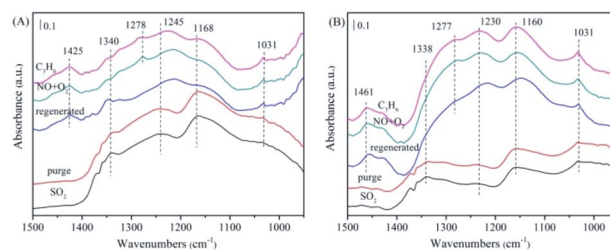

Fig. 11 The *in situ* FTIR spectra of the NiAlO and 5% MnNiAlO catalysts after washed regeneration reacting with NO + O$_2$ and C$_3$H$_6$ at 200 °C. (A) NiAlO; (B) 5% MnNiAlO.

activated to form a more thermally stable sulfate species adsorbed on the catalyst, resulting in more severe clogging. After the introduction of NO/O$_2$, the characteristic peak (at 1278 cm^{-1}) belonging to monodentate nitrates appeared, and after introduction of C$_3$H$_6$, the peak disappeared. It is shown that the method of washing regeneration can restore partial activity of catalyst.

For 5% MnNiAlO catalyst (Fig. 11(B)), the peaks of sulfite (1031 cm^{-1}) decreased, whereas that of sulfate at 1160 cm^{-1} increased. In addition, 5% MnNiAlO catalyst had fewer types of sulfate species and smaller quantities. More important, the sulfate peak at 1338 cm^{-1} disappeared. After injecting NO/O$_2$, it also appeared the characteristic peak at 1277 cm^{-1}, attributing to monodentate nitrate. After introduction of C$_3$H$_6$, the monodentate nitrate disappeared. According to the results, the method of washing regeneration can expose more active sites so as to facilitate the progress of adsorption and activation of SO$_2$. It also can restore the ability of reaction between sulfate/sulfite and C$_3$H$_6$ of all catalysts, showing remarkable recovery ability over the MnNiAlO catalyst.

3.6. Study on the poisoning mechanism of S

XPS spectra were employed to further characterize the surfaces. The XPS spectra of Mn 2p are illustrated in Fig. 12(A). After a peak fitting deconvolution, the Mn 2p XPS spectra could be separated into two peaks of Mn^{2+} (639.8 eV) and Mn^{4+} (645.5 eV).[37] From the results of XPS analysis, it is clearly to find that the quantity of Mn^{4+} in the S-poisoned catalyst was lower than that in the fresh catalyst. In contrast, in the regenerated catalyst, the Mn^{4+} peak intensity was greater. These results indicate that S poisoning resulted in a distinct decrease of surface Mn^{4+}. It is proposed that high Mn^{4+} concentration could promote the oxidation of NO to NO$_2$, while SO$_2$ could be oxidized to SO$_4^{2-}$ using the oxygen supplied by Mn^{4+} species, leading to the partial reduction of Mn^{4+}.[38]

The O 1s spectra (Fig. 12(B)) can be deconvoluted with two peaks, referred to as the surface chemisorbed oxygen O$_A$ (532.0 eV), and lattice oxygen O$_L$ (530.6 eV), respectively.[39] It is well known that O$_A$ is much more active than O$_L$ in oxidation reactions because of its higher mobility.[40] Liu *et al.*[41] showed that O$_A$ was the most active oxygen species which were deciding to the oxidation of NO, then the SCR reaction was enhanced by "fast SCR" reaction. We compared the quantity of O$_A$ *via* calculating

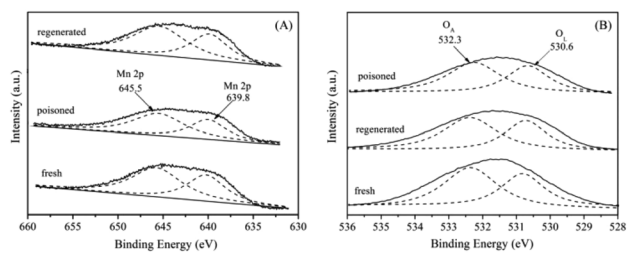Fig. 10 The FTIR spectra of the NiAlO and 5% MnNiAlO catalysts after thermal regeneration at 200 °C. (A) NiAlO; (B) 5% MnNiAlO.

Fig. 12 XPS spectra of the fresh, S-poisoned and washing regenerated 5% MnNiAlO catalysts. (A) Mn XPS spectra; (B) O XPS spectra.

Fig. 14 (A) FTIR spectra of pyridine adsorption on 5% MnNiAlO catalysts. (B) Brønsted acid sites quantification of NiAlO and MnNiAlO catalysts.

the ratio of peak area: $O_A/(O_A + O_L)$. It can be seen that the $O_A/(O_A + O_L)$ ratio over SO_2 poisoned sample (59.1%) was less than that of fresh sample (65.9%), because surface chemisorbed oxygen could be consumed by SO_2. Further, the ratio of $O_A/(O_A + O_L)$ was recovered to 62.3% after washing regenerating, indicating that washing regeneration can restore partial surface chemisorbed oxygen of catalyst.

To further analysis the poisoning mechanism of the 5% MnNiAlO catalyst, we performed FTIR experiments on the fresh, S-poisoned and washing regenerated catalysts (Fig. 13). One peak appeared for the S-poisoned catalyst located at 1129 cm^{-1}, which can be attributed to sulfate species. Importantly, there is an obvious decrease in the intensity of 1129 cm^{-1} peak over the washing regenerated samples. The results indicate that most of sulfate species deposited on the S-poisoned catalyst could be removed by water washing.

To distinguish the acidity styles and acid sites of the catalysts, the Py-IR characterization was performed. As shown in Fig. 14(A), the bands attributed to pyridine adsorbed on Brønsted acid sites (1576 cm^{-1}) and Lewis acid sites (1491 and 1604 cm^{-1}) were detected. Another band (1448 cm^{-1}) due to pyridine interacting with both Brønsted and Lewis acid sites was also observed.[42,43] Comparatively, the amount of Brønsted acid sites on fresh catalyst declined dramatically with SO_2 poisoning treatment; whereas the amount of Lewis acid sites showed a slight increase.

This result implies that SO_2 can increase the Lewis acid sites but decrease the Brønsted acid sites. Previous studies reported
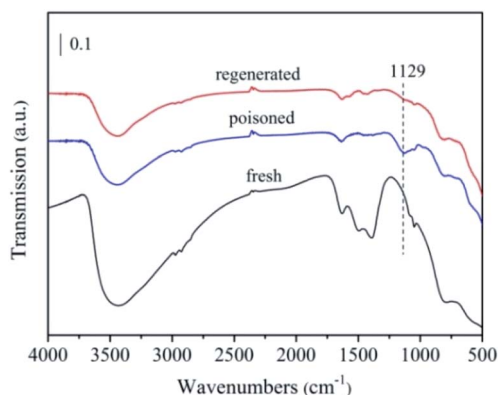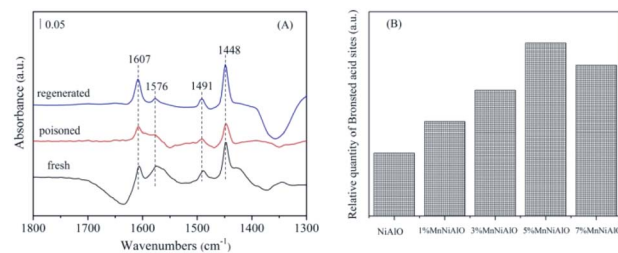
that Brønsted acid sites are important SCR active sites for NO reduction.[44] The SO_2-poisoned sample exhibited relatively weak NO adsorption strength and NO reduction ability, which agreed with the results of the FTIR spectra (Fig. 11). In addition, the Brønsted acid sites could be recovered to almost the same level as the fresh catalyst after washing regenerating. Meanwhile, from the Brønsted acid sites quantification analysis (Fig. 14(B)), we can see that the amount of Brønsted acid sites over MnNiAlO catalysts were more abundant than that of NiAlO sample.

On the basis of the above studies, some possible reaction mechanisms for improved NO reduction in the absence and presence of SO_2 are provided as follows. On one hand, the NiAlO catalyst shows relatively poor activity owing to the weak redox, oxygen storage/release ability and less surface Brønsted acid sites, which lead to insufficient accumulation of adNO$_x$ and generation of $C_xH_yO_z$ species during C_3H_6-SCR. In the case of MnNiAlO catalysts, Mn doping enhances the Brønsted acid sites and active oxygen groups, and improves the redox property by the redox cycle ($Ni^{3+} + Mn^{2+} \leftrightarrow Ni^{2+} + Mn^{4+}$). Subsequently, the reaction intermediates and the reactivity between $C_xH_yO_z$ species and nitrite/nitrate species are promoted, which contribute to excellent C_3H_6-SCR performance. On the other hand, in the presence of SO_2, for the NiAlO catalyst, SO_2 strongly competes with NO to adsorb on the catalyst surface to form stable $NiSO_4$ or $Al_2(SO_4)_3$ compounds, which can impair the amount of active sites and decline the occurrence of C_3H_6-SCR reactions. After Mn addition, the SO_2-poisoned MnNiAlO catalysts generate much greater absorbed NO species than over SO_2-poisoned NiAlO sample. SO_2 reacts with Mn in the outer layer from the formation of $MnSO_4$ which can protect the reaction active sites Ni–O–Al. It has been demonstrated that Mn addition gives rise to minor formation of sulfate after exposure to SO_2 and improves the resistance of catalyst towards SO_2. Furthermore, the competitive adsorption phenomenon is dramatically inhibited over MnNiAlO samples due to their nitrite/nitrate species are more abundant and stable in comparison to NiAlO catalyst. As a result, the C_3H_6-SCR of NO in the presence of SO_2 has been significantly improved.

4. Conclusions

The various manganese amounts loaded NiAl hydrotalcite-like compounds were developed for selective catalytic reduction of NO with C_3H_6. Among them, 5% MnNiAlO catalyst exhibited

Fig. 13 FTIR spectra of the fresh, S-poisoned and washing regenerated 5% MnNiAlO catalysts.

more than 95% and 88% NO_x conversion in the presence and absence of SO_2, respectively. The Mn doping enhances the Brønsted acid sites and surface active oxygen groups, and improves the redox property by the redox cycle ($Ni^{3+} + Mn^{2+} \leftrightarrow Ni^{2+} + Mn^{4+}$). *In situ* FTIR experiments showed that loading Mn on catalysts could improve the reaction intermediates and promote the reactivities between $C_xH_yO_z$ species and nitrite/nitrate species, which contributes to excellent C_3H_6-SCR performance. In addition, in the presence of SO_2, the XPS and FTIR results showed that sulfur species and nitrogen species were deposited on the catalyst surface, which made the catalyst poisoned. The MnNiAlO samples can give rise to minor formation of sulfate and inhibit the competitive adsorption effectively due to their nitrite/nitrate species are more abundant and stable. Finally, water washing method showed best performance on the regeneration of deactivated catalysts. The Brønsted acid sites could be recovered to almost the same level as the fresh catalyst after washing regenerating.

Conflicts of interest

There are no conflicts to declare.

Acknowledgements

References

1 S. X. Cai, J. Liu, K. Zha, H. Li, L. Shi and D. Zhang, *Nanoscale*, 2017, **9**, 5648–5657.

2 T. Boningari and P. G. Smirniotis, *Chem. Eng.*, 2016, **13**, 133–141.

3 X. Y. Li, G. Lu, Z. P. Qu, D. K. Zhang and S. M. Liu, *Appl. Catal., A*, 2011, **398**, 82–87.

4 W. Yang, R. D. Zhang, B. H. Chen, D. Duprez and S. Royer, *Environ. Sci. Technol.*, 2012, **46**, 11280–11288.

5 I. Sobczak, K. Musialska, H. Pawlowski and M. Ziolek, *Catal. Today*, 2011, **176**, 393–398.

6 S. Putluru, L. Schill, A. Jensen, B. Siret, F. Tabaries and R. Fehrmann, *Appl. Catal., B*, 2015, **165**, 628–635.

7 L. Fin, X. D. Wu and S. Liu, *Chem. Eng.*, 2013, **226**, 105–112.

8 R. Jin, Y. Liu, Z. B. Wu, H. Q. Wang and T. T. Gu, *Chemosphere*, 2010, **78**, 1160–1166.

9 Q. Li, M. Meng, H. Xian, N. Tsubaki, X. G. Li and Y. Xie, *Environ. Sci. Technol.*, 2010, **44**, 4747–4752.

10 Z. L. Zhang, Y. Zhang, Q. Y. Su, Z. P. Wang, Q. Li and X. Y. Gao, *Environ. Sci. Technol.*, 2010, **44**, 8254–8258.

11 L. Xue, H. He and C. Liu, *Environ. Sci. Technol.*, 2009, **43**, 890–895.

12 X. Wu, R. N. Wang, Y. L. Du and X. J. Li, *New J. Chem.*, 2019, **43**, 2640–2648.

13 L. F. Zhang, X. L. Zhang, S. S. Lv, X. P. Wu and P. M. Wang, *RSC Adv.*, 2015, **5**, 82952–82959.

14 Z. B. Wu, R. B. Jin, H. Q. Wang and Y. Liu, *Catal. Commun.*, 2009, **10**, 935–939.

15 Y. Peng, D. Wang, B. Li, C. Z. Wang, J. H. Li, J. Crittenden and J. M. Hao, *Environ. Sci. Technol.*, 2017, **51**, 11943–11949.

16 Y. Peng, W. Z. Si, X. Li, J. Chen, J. H. Li, J. Crittenden and J. M. Hao, *Environ. Sci. Technol.*, 2016, **50**, 9576–9582.

17 H. Zhou, Y. X. Su, W. Y. Deng and F. C. Zhong, *Environ. Sci. Technol.*, 2016, **39**, 93–100.

18 Y. J. Kim, H. J. Kwon, I. S. Nam, J. W. Choung, J. K. Kil, H. J. Kim, M. S. Cha and G. K. Yeo, *Catal. Today*, 2010, **151**, 244–250.

19 W. Tian, H. S. Yang, X. Y. Fan and X. B. Zhang, *J. Hazard. Mater.*, 2011, **188**, 105–109.

20 S. C. Deng, T. T. Meng, B. L. Xu, F. Gao, Y. H. Ding, L. Yu and Y. N. Fan, *ACS Catal.*, 2016, **6**, 5807–5815.

21 L. Zhao, X. Y. Li and J. Zhao, *Chem. Eng. J.*, 2013, **223**, 164–171.

22 L. Chmielarz, P. Kustrowski, A. R. Lasocha and R. Dziembaj, *Thermochim. Acta*, 2002, **395**, 225–236.

23 J. S. Valente, M. S. Cantu, J. G. H. Cortez, R. Montiel, X. Bokhimi and E. López-Salinas, *J. Phys. Chem. C*, 2007, **111**, 642–651.

24 N. T. Nivangune and V. V. Ranade, *Catal. Lett.*, 2017, **147**, 2558–2569.

25 A. C. Vieira, R. L. Moreira and A. Dias, *J. Phys. Chem. C*, 2009, **113**, 13358–13368.

26 A. Djaidja, S. Libs and A. Kiennemann, *Catal. Today*, 2006, **113**, 194–200.

27 K. Ramesh, L. Chen and F. Chen, *Catal. Today*, 2008, **131**, 477–482.

28 Z. Q. Liu, J. H. Li, M. Buettner, R. V. Ranganathan, M. Uddi and R. Wang, *ACS Appl. Mater. Interfaces*, 2019, **11**, 17035–17049.

29 L. Chen, J. H. Li and M. Ge, *Environ. Sci. Technol.*, 2010, **44**, 9590–9596.

30 A. L. Goodman, E. T. Bernard and V. H. Grassian, *J. Phys. Chem. A*, 2001, **105**, 6443–6457.

31 T. I. Halkides, D. I. Kontaridis and X. E. Verykios, *Catal. Today*, 2002, **73**, 213–221.

32 H. Zhou, Y. X. Su, W. Y. Liao and F. C. Zhong, *Fuel*, 2016, **182**, 352–360.

33 A. L. Goodman, P. Li, C. R. Usher and V. H. Grassian, *J. Phys. Chem. A*, 2001, **105**, 6109–6120.

34 Y. Liu, E. Lotero and J. G. Goodwin, *Appl. Catal., A*, 2007, **331**, 138–148.

35 V. G. Milt, M. A. Ulla and E. E. Miro, *Appl. Catal., B*, 2005, **57**, 13–21.

36 L. Zhao, J. Duan, S. W. Yang, X. Y. Li, Q. F. Liu and C. J. Martyniuk, *Sep. Purif. Technol.*, 2018, **207**, 231–239.

37 C. Z. Sun, H. Liu, W. Chen, D. Z. Chen, S. H. Yu, A. N. Liu, L. Dong and S. Feng, *Chem. Eng. J.*, 2018, **347**, 27–40.

38 C. Fang, D. Zhang, S. Cai, L. Zhang, L. Huang, H. Li, P. Maitarad, L. Shi, R. Gao and J. Zhang, *Nanoscale*, 2013, **5**, 9199–9207.

39 K. J. Lee, P. A. Kumar, M. S. Maqbool, K. N. Rao, K. H. Song and H. P. Ha, *Appl. Catal., B*, 2013, **142–143**, 705–717.

40 S. Zhan, H. Zhang, Y. Zhang, Q. Shi, Y. Li and X. Li, *Appl. Catal., B*, 2017, **203**, 199–209.

41 F. Liu, H. He and Y. Ding, *Appl. Catal., B*, 2009, **93**, 194–204.

42 N. Jagtap, S. B. Umbarkar and P. Miquel, *Appl. Catal., B*, 2009, **90**, 416–425.

43 D. Yuan, X. Y. Li, Q. D. Zhao, J. J. Zhao and S. M. Liu, *Appl. Catal., A*, 2013, **451**, 176–183.

44 L. Kang, L. P. Han, J. B. He, H. R. Li, T. T. Yan, G. R. Chen, J. P. Zhang, L. Y. Shi and D. S. Zhang, *Environ. Sci. Technol.*, 2019, **53**, 938–945.